Probing the single-particle behavior above ^{132}Sn via electromagnetic moments of ^{133,134}Sb and $N = 82$ isotones

S. Lechner ,[1,2,*] Z. Y. Xu,[3,4] M. L. Bissell,[5] K. Blaum,[6] B. Cheal ,[7] G. De Gregorio ,[8,9] C. S. Devlin ,[7] R. F. Garcia Ruiz,[1,†] A. Gargano ,[8] H. Heylen,[1] P. Imgram ,[10] A. Kanellakopoulos ,[3,‡] Á. Koszorús,[3,§] S. Malbrunot-Ettenauer,[1] R. Neugart,[6,11] G. Neyens ,[1,3] W. Nörtershäuser ,[10] P. Plattner,[1,12] L. V. Rodríguez ,[6,13,‖] X. F. Yang,[14] and D. T. Yordanov[13]

[1]*Experimental Physics Department, CERN, CH-1211 Geneva 23, Switzerland*
[2]*Technische Universität Wien, AT-1040 Wien, Austria*
[3]*Instituut voor Kern- en Stalingsfysica, KU Leuven, B-3001, Leuven, Belgium*
[4]*Department of Physics and Astronomy, University of Tennessee, Knoxville, Tennessee 37996, USA*
[5]*School of Physics and Astronomy, University of Manchester, Manchester M13 9PL, England, United Kingdom*
[6]*Max-Planck-Institut für Kernphysik, D-69117 Heidelberg, Germany*
[7]*Oliver Lodge Laboratory, University of Liverpool, Liverpool L69 7ZE, England, United Kingdom*
[8]*Istituto Nazionale di Fisica Nucleare, Sezione di Napoli, 80126 Napoli, Italy*
[9]*Dipartimento di Matematica e Fisica, Università degli Studi della Campania Luigi Vanvitelli, 81100 Caserta, Italy*
[10]*Institut für Kernphysik, Technische Universität Darmstadt, D-64289 Darmstadt, Germany*
[11]*Institut für Kernchemie, Universität Mainz, D-55128 Mainz, Germany*
[12]*Universität Innsbruck, AT-6020 Innsbruck, Austria*
[13]*Université Paris-Saclay, Centre National de la Recherche Scientifique IN2P3, IJCLab, 91405 Orsay, France*
[14]*School of Physics and State Key Laboratory of Nuclear Physics and Technology, Peking University, Beijing 10871, China*

(Received 28 April 2021; accepted 26 May 2021; published 2 July 2021)

Magnetic and quadrupole moments of the $7/2^+$ ground state in ^{133}Sb and the (7^-) isomer in ^{134}Sb have been measured by collinear laser spectroscopy to investigate the single-particle behavior above the doubly magic nucleus ^{132}Sn. The comparison of experimental data of the $7/2^+$ states in ^{133}Sb and neighboring $N = 82$ isotones to shell-model calculations reveals the sensitivity of magnetic moments to the splitting of the spin-orbit partners $\pi 0g_{9/2}$ and $\pi 0g_{7/2}$ across the proton shell closure at $Z = 50$. In contrast, quadrupole moments of the $N = 82$ isotones are insensitive to cross-shell excitations, but require the full proton model space from $Z = 50$ to 82 for their accurate description. In fact, the linear trend of the quadrupole moment follows approximately the expectation of the seniority scheme when filling the $\pi 0g_{7/2}$ orbital. As far as the isomer in ^{134}Sb is concerned, its electromagnetic moments can be perfectly described by the additivity rule employing the moments of ^{133}Sb and ^{133}Sn, respectively. These findings agree with shell-model calculations and thus confirm the weak coupling between the valence proton and neutron in ^{134}Sb.

DOI: 10.1103/PhysRevC.104.014302

I. INTRODUCTION

Out of the over 3000 atomic nuclei discovered so far [1], only about ten represent nuclides with closed nuclear shells for both protons and neutrons. Such rare exemplars, found at the traditional shell closures $Z, N = 2$, 8, 20, 28, 50, 82, or 126, are called doubly magic nuclei. Studies of electromagnetic moments in the region of doubly magic species contribute to our understanding of the single-particle behavior predicted by the spherical shell model [2]. In particular, magnetic dipole moments of systems with one proton on top of a doubly magic nucleus are sensitive to meson-exchange currents and core-polarization effects [3,4]. Moreover, deviations from the Schmidt moment give insights on the purity of the nuclear configuration, while electric quadrupole moments allow the investigation of second order core-polarization effects. Examples for this can be found in ^{41,49}Sc [4] (^{40,48}Ca

*simon.lechner@cern.ch
†Present address: Massachusetts Institute of Technology, Cambridge, MA 02139, USA.
‡Present address: HEPIA Geneva, HES-SO, 1202 Geneva, Switzerland.
§Present address: Oliver Lodge Laboratory, Oxford Street, University of Liverpool, Liverpool L69 7ZE, England, United Kingdom.
‖Present address: Experimental Physics Department, CERN, CH-1211 Geneva 23, Switzerland.

core + proton), ^{57,69}Cu [5] (^{56,68}Ni core + proton), and ^{209}Bi [2] (^{208}Pb core + proton).

Another candidate is ^{133}Sb with one proton in the $0g_{7/2}$ orbital on top of a doubly magic ^{132}Sn core. Despite its large N/Z ratio, the magicity of ^{132}Sn was already firmly established [6,7]. The latest evidence was added by laser spectroscopy of ^{133}Sn [8], where it was shown that the electromagnetic moments of ^{133}Sn can be well described in a single-particle picture with the valence neutron in the $1f_{7/2}$ orbital on top of a ^{132}Sn core. A similar behavior would be expected for ^{133}Sb. However, in Ref. [3] a rather large deviation of the magnetic moment to the Schmidt value was found. This deviation was mainly attributed to meson-exchange currents and first-order core-polarization effects. The latter is driven by the interplay of the spin-orbit partners $0g_{9/2}$ and $0g_{7/2}$ ($j = l \pm s$), which belong to different shells. An analogous behavior was observed in the equivalent magnetic moment of ^{209}Bi with a $0h_{9/2}$ proton above a doubly magic ^{208}Pb core [2].

As a missing piece in this discussion, the quadrupole moment of ^{133}Sb has not been measured so far. Furthermore, electromagnetic moments of ^{134}Sb (^{132}Sn + one proton + one neutron) would allow for further investigations of single-particle behavior above ^{132}Sn, but are unknown. The objective of this research was therefore to measure the electromagnetic moments of ^{133,134}Sb with high-resolution laser spectroscopy in order to establish a better understanding of nuclear structure above the doubly magic nucleus ^{132}Sn. To extend the perspective, electromagnetic moments of $N = 82$ isotones above ^{133}Sb with protons filling the $0g_{7/2}$ orbital are included in the discussion. Simple trends in this isotonic chain can be qualitatively explained by using the seniority scheme for a single-orbital configuration. Additionally, state-of-the-art shell-model calculations are employed for a more quantitative understanding. This theoretical work illustrates the importance of proton excitations across the $Z = 50$ shell for the description of magnetic moments in $N = 82$ isotones, while they do not affect quadrupole moments. On the other hand, the moments of the (7^-) isomer in ^{134}Sb are well described by the weak coupling of the valence proton of ^{133}Sb and the valence neutron of ^{133}Sn, providing a textbook example for the additivity rule of electromagnetic moments.

II. EXPERIMENT

The experiment was carried out at the radioactive ion-beam facility ISOLDE-CERN [9], where a large variety of nuclides can be synthesized by high-energy protons impinging on a thick target. Neutron-rich antimony (Sb) isotopes were formed by directing the protons onto a neutron converter to enable neutron-induced fission in a UCx target. Subsequently, atomic Sb was selectively laser ionized [10], electrostatically accelerated to 50 keV, magnetically mass separated, and accumulated in a buffer-gas filled radio-frequency quadrupole cooler and buncher [11]. Cooled ion bunches with a temporal width of around 6 μs were reaccelerated to 50 keV and sent to the COLLAPS beam line [12]. There, the ions were neutralized in a potassium-filled charge-exchange cell [13,14] as depicted in Fig. 1. The atom bunches were then collinearly overlapped with a narrow-band continuous-wave laser beam. Photons, emitted after resonant excitation of the Sb atoms, were detected by four photomultiplier tubes.

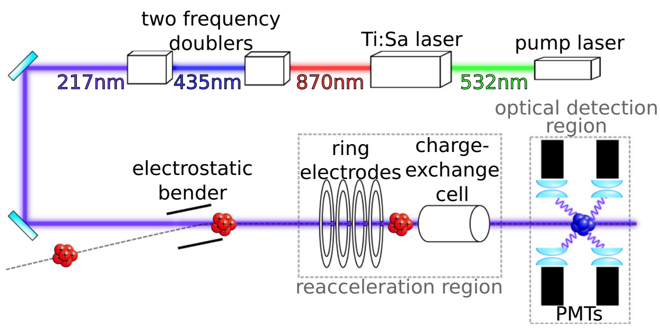

FIG. 1. Overview of the COLLAPS setup. The laser system consisted of a Ti:Sa laser, pumped by a frequency-doubled Nd:YAG laser and producing infrared light at 870 nm. The fundamental light was frequency doubled twice to obtain a laser beam at 217 nm. Ion bunches (red) from ISOLDE were guided by a 10° electrostatic bender onto the axis of the experiment, where they were collinearly overlapped with the laser beam. In the reacceleration region, consisting of four ring electrodes and the charge-exchange cell (CEC), the final beam energy was defined. Ions were neutralized in the CEC by collisions with potassium. The atom bunches (blue) then entered the optical detection region. Photons, emitted after resonant excitation of the Sb atoms, were collected by pairs of aspheric lenses and detected by four photomultiplier tubes (PMTs).

In order to obtain hyperfine spectra, the Doppler-shifted laser frequency observed by the fast moving atoms was scanned by varying the floating voltage of the charge-exchange cell, which resulted in a change of the longitudinal atom velocity. Hence, the laser frequency in the laboratory frame was kept fixed, which enabled faster measurements together with an increased laser stability. The large beam energy E, compared to its energy spread $\delta E \approx 3$ eV, allowed high-resolution measurements of the hyperfine structure with linewidths of about 80 MHz by minimizing the Doppler broadening according to $\delta\nu_{\mathrm{D}} \propto \delta E/\sqrt{E}$ [15]. Furthermore, the bunched structure of the beam allowed a gate to be placed on the photon counting for the time when the atoms passed the photon detectors, vastly improving the signal-to-background ratio compared to continuous beams [16,17]. More details on collinear laser spectroscopy as performed at COLLAPS can be found in the review of Neugart *et al.* [12].

The atomic transition $5s^25p^3\ ^4S_{3/2} \rightarrow 5s^25p^26s\ ^4P_{3/2}$ was probed by laser light at a wavelength of 217 nm. This transition was chosen due to its sensitivity to magnetic and quadrupole moments. The laser beam was produced by frequency quadrupling the fundamental of a Ti:Sa laser (Matisse 2TS) as depicted in Fig. 1. The stability of the laser frequency was ensured by locking the fundamental of the Ti:Sa laser to a wavelength meter (HighFinesse WSU10). The wavelength meter itself was calibrated once per minute to a diode laser (Toptica DLPRO780), which was locked to the $F = 2 \rightarrow F = 3$ hyperfine transition of the D1 line in ^{87}Rb.

Hyperfine spectra of ^{133,134}Sb have been recorded for the first time, in addition to those of the two stable Sb isotopes, ^{121,123}Sb. The resulting data were analyzed with the SATLAS package [18], using χ^2 minimization fitting routines. The line shape is described by a Voigt profile and two side peaks. These account for the asymmetric peak shape caused by energy losses during the charge-exchange process [19,20]. As fitting function, Eqs. (20) and (21) from Ref. [18] were employed, which yielded the hyperfine parameters A and B for the lower (l) and upper (u) level of the transition. Since B_l is too small to be properly resolved, the ratio of B_u/B_l was determined for the two stable isotopes ^{121}Sb and ^{123}Sb by varying B_l within the range of the high-precision values obtained from atomic-beam measurements [21]. This yielded a B ratio of 128.6(6), which was set as a constraint for the analysis of ^{133}Sb and ^{134}Sb. The hyperfine peak intensities were free parameters in the fit.

The magnetic moment μ and the quadrupole moment Q were derived from the hyperfine parameters with respect to the reference isotope ^{123}Sb:

$$\mu = \mu_{\text{ref}} \frac{AI}{A_{\text{ref}} I_{\text{ref}}} \tag{1}$$

and

$$Q = Q_{\text{ref}} \frac{B}{B_{\text{ref}}}. \tag{2}$$

This approach is valid as long as the ratios between the hyperfine values from lower and upper levels are constant. This holds true for B, but is not fully correct for magnetic moments. Variations of the magnetic hyperfine field over the nuclear volume can cause a hyperfine anomaly (hfa) Δ, which can have a sizable influence on the magnetic moment. Thus, Eq. (1) has to be adapted to

$$\mu = \mu_{\text{ref}} \frac{AI}{A_{\text{ref}} I_{\text{ref}}} (1 + \Delta). \tag{3}$$

For the atomic ground state of antimony the hfa was measured to be $^{121}\Delta^{123} = -0.317(3)\%$ [21] and, therefore, cannot be neglected. To evaluate the approximate size of the hfa for ^{133}Sb and ^{134}Sb with respect to ^{123}Sb, simple calculations using a single-particle model [22,23] were carried out. These calculations showed that the hfa is negligible between ^{123}Sb and ^{133}Sb, as expected since both isotopes are in the same nuclear configuration. On the other hand, the calculations yield $^{134}\Delta^{123} \approx 0.5\%$, which has to be taken into account. Since more reliable calculations are difficult and not available at the moment, the hfa from the single-particle model is presently the best estimate. In order to account for uncertainties in this single-particle model, the derived hfa value is multiplied by a factor of 2 (thus, $^{134}\Delta^{123} \approx 1\%$) and added as a systematic uncertainty to the magnetic moment of ^{134}Sb, which is calculated via Eq. (1). These calculations are only valid for the lower atomic level. Therefore, only A_l is used for the determination of the magnetic moments except for ^{133}Sb, where we expect a negligible hfa with respect to ^{123}Sb in the upper atomic level as well. Details about the hfa calculations can be found in Ref. [24].

III. RESULTS

The spectra of ^{133}Sb and ^{134}Sb are shown in Fig. 2 together with their hyperfine level scheme. For ^{133}Sb, the spin of the ground state was already firmly assigned to $I = 7/2$ [26] and is a consequence of the valence proton in the $0g_{7/2}$ orbital. This assignment is confirmed by this paper as shown in Fig. 3(a). For ^{134}Sb, only the isomer was observed in the hyperfine spectrum [see Fig. 2(b)]. This isomer is tentatively assigned with a spin/parity of $I^\pi = (7^-)$ and has an excitation energy of 0.279(1) MeV [27]. In the present analysis it was not possible to make a distinction between $I = 7$, 8, and 9 [see Fig. 3(b)], while all other spins can be excluded. However, in order to have $I = 8$, the isomer of ^{134}Sb would need to be in a $\pi 0g_{7/2} \times \nu 0h_{9/2}$ configuration. This seems improbable since

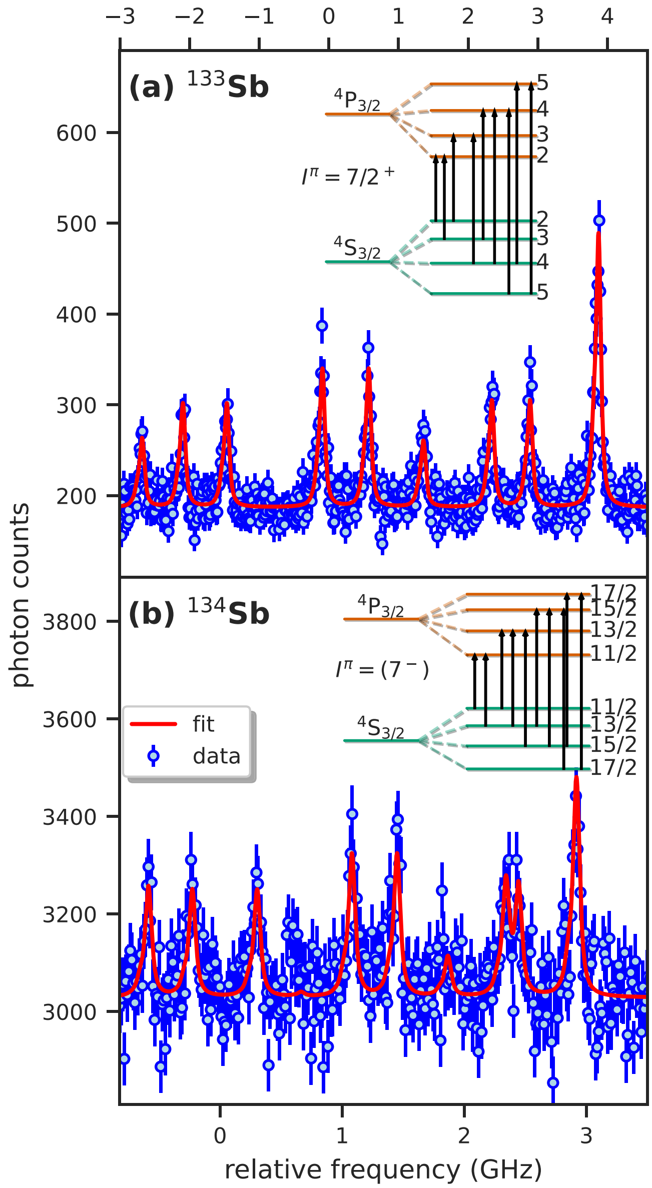

FIG. 2. Hyperfine spectra of (a) the $7/2^+$ ground state of ^{133}Sb and (b) the (7^-) isomeric state of ^{134}Sb in the $5s^2 5p^3\ ^4S_{3/2} \rightarrow 5s^2 5p^2 6s\ ^4P_{3/2}$ transition. The frequency is given as an offset from the transition frequency [45 945.340(5) cm^{-1} [25]]. A scheme of the hyperfine splitting is shown, where each arrow is connected to one hyperfine peak. While the spectrum of ^{133}Sb was obtained in around 10 min, the one for ^{134}Sb took more than 7 h due to large isobaric contamination.

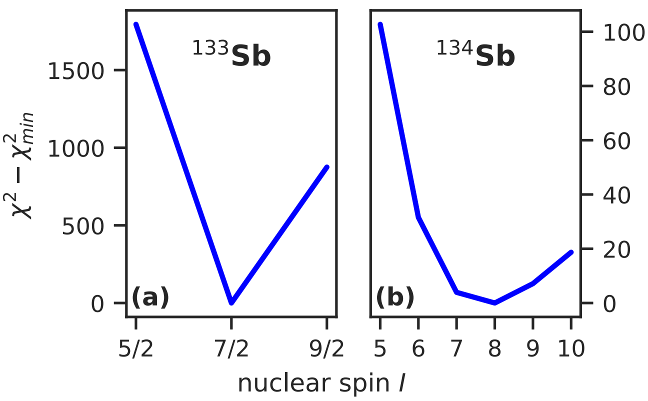

FIG. 3. Spin assignment of **(a)** ^{133}Sb and **(b)** ^{134}Sb with the χ^2 from the data fit as a function of the nuclear spin. In the case of ^{133}Sb, only $I = 7/2$ gives a reasonable result. On the other hand, ^{134}Sb has a minimum at $I = 8$, but the difference in χ^2 to $I = 7$ and $I = 9$ is too small for a clear spin assignment. However, other possibilities can be excluded. See text for details.

in ^{133}Sn the $\nu 0h_{9/2}$ state is around 1.5 MeV above the $\nu 1f_{7/2}$ ground state. Similar arguments can be made to exclude $I = 9$. Therefore, $I = 7$ is used in the following as also suggested in Ref. [27] and supported by shell-model calculations in this paper, which place the 7^- and 8^- states at excitation energies of 0.408 and 1.67 MeV, respectively.

Table I gives an overview of the measured hyperfine parameters in comparison to known values in literature of the stable isotopes ^{121}Sb and ^{123}Sb. With the exception of A_l in ^{123}Sb, excellent agreement with literature is obtained. A difference of close to 2σ in $A_\mathrm{l}(^{123}\mathrm{Sb})$ is seen. We found no obvious reason to doubt our result or the literature value. In the end, the 2σ level does not exclude compatibility of the two results. Due to its higher precision, A_l from Ref. [21] is used as reference value to derive the magnetic moments.

From the values of the hyperfine parameters in Table I, together with reference values from ^{123}Sb of $A_\mathrm{l} = -162.451(3)$ MHz [21] and $B_\mathrm{u} = -602.9(7)$ MHz (from this paper) the magnetic and quadrupole moments of ^{121}Sb, ^{133}Sb, and ^{134}Sb given in Table II were calculated via Eqs. (1) and (2), respectively. In the case of ^{133}Sb, the magnetic moment was additionally derived for the upper atomic level and the weighted average from both levels is given in Table II. Correlations between A_l and A_u of ^{133}Sb, which would slightly reduce the uncertainty, are not included in our final value. The very good agreement with literature in stable ^{121}Sb gives confidence in our results for the radioactive isotopes. Note that the uncertainty on Q_ref, taken from Ref. [30], limits the precision of the new quadrupole moments in this paper.

There is a small discrepancy between the magnetic moment of ^{133}Sb from this paper and from Ref. [3], in which Stone *et al.* employed the technique of nuclear magnetic resonance on oriented nuclei, which relies on the magnetic hyperfine field B_hf of Sb in iron. They used B_hf from Ref. [33], while applying B_hf from Ref. [34] would yield good agreement with our value. Hence, the deviation arises most probably from the choice of B_hf.

IV. THEORY

A. Single-particle considerations

For a single-orbital configuration with n protons, the magnetic moment of seniority-1 states can be written as [2,35]

$$\mu(j^n) = \mu_\mathrm{SP} = \begin{cases} \left(j - \frac{1}{2}\right)g_l + \frac{g_s}{2}, & \text{for } j = l + \frac{1}{2} \\ \frac{j}{j+1}\left[\left(j + \frac{3}{2}\right)g_l - \frac{g_s}{2}\right], & \text{for } j = l - \frac{1}{2} \end{cases}, \tag{4}$$

where j and l are the total and orbital angular momenta characterizing the orbital and μ_sp stands for the single-particle moment, also called the Schmidt value. The quantities g_l and g_s are the orbital and spin g factors for the proton, the free values of which are $g_l = 1$ and $g_s = 5.585\,694\,689\,3(16)$ [36,37], respectively. However, effective g factors are usually introduced in single-j as well as in multi-j models to account for the neglected degrees of freedom, namely, the remaining nucleons as well as the truncation of the Hilbert space.

In the case of odd-odd nuclei with a rather pure configuration (e.g., ^{134}Sb), the magnetic moment of a state with spin I can be estimated from a composition of the valence proton and neutron via an additivity rule [2]:

$$\mu(I) = \frac{I}{2}\left[\frac{\mu(I_\pi)}{I_\pi} + \frac{\mu(I_\nu)}{I_\nu} + \left(\frac{\mu(I_\pi)}{I_\pi} - \frac{\mu(I_\nu)}{I_\nu}\right)\frac{I_\pi(I_\pi+1) - I_\nu(I_\nu+1)}{I(I+1)}\right]. \tag{5}$$

TABLE I. Hyperfine parameters of ^{121,123,133,134}Sb in comparison to literature. Note that B_l of ^{121,123}Sb was fixed to the given literature values, while B_l of ^{133,134}Sb was derived from B_u using the B ratio $B_\mathrm{u}/B_\mathrm{l} = 128.6(6)$, which was fixed in the fit of the hyperfine spectra. See text for details.

		A_l (MHz)		A_u (MHz)		B_l (MHz)		B_u (MHz)	
	I^π	Exp.	Lit.	Exp.	Lit.	Exp.	Lit.	Exp.	Lit.
^{121}Sb	$5/2^+$	−299.0(3)	−299.034(4) [21]	523.8(5)	519(6) [28]		−3.68(2) [21]	−471.1(17)	−480(15) [28]
^{123}Sb	$7/2^+$	−162.59(8)	−162.451(3) [21]	285.20(8)	282(4) [29]		−4.67(3) [21]	−602.9(7)	
^{133}Sb	$7/2^+$	−196.1(2)		343.7(2)		−2.06(2)		−265(2)	
^{134}Sb	(7^-)	−55.7(3)		97.7(3)		−3.24(5)		−416(7)	

TABLE II. Magnetic and quadrupole moments of ^{121,123,133,134}Sb in comparison to literature where ^{123}Sb was used as reference to derive the moments of the other isotopes. Literature magnetic moments given here are obtained from a reevaluation in Ref. [31], while the second citation indicates the original measurement.

	I^π	$\mu_{\rm exp}$ ($\mu_{\rm N}$)	$\mu_{\rm lit}$ ($\mu_{\rm N}$)	$Q_{\rm exp}$ (b)	$Q_{\rm lit}$ (b)
^{121}Sb	$5/2^+$	3.357(4)[a]	3.3580(16) [31,32]	−0.541(11)	−0.543(11) [30]
^{123}Sb	$7/2^+$		2.5457(12) [31,32]		−0.692(14) [30]
^{133}Sb	$7/2^+$	3.070(2)	3.00(4) [3,31]	−0.304(7)	
^{134}Sb	(7^-)	1.745(8){17}[b]		−0.477(12)	

[a]A hyperfine anomaly of −0.317(3)% from Ref. [21] is included in this value.
[b]The calculated hyperfine anomaly is denoted in curly brackets as a systematic uncertainty.

For ^{134}Sb as an example, the proton and neutron moments are taken from ^{133}Sb and ^{133}Sn, respectively.

Similar considerations can be made for quadrupole moments. For a single-j orbital containing n particles, the quadrupole moment of seniority-1 states can be expressed as [35,38]

$$Q(j^n) = Q_{\rm SP}\frac{2j+1-2n}{2j-1}, \tag{6}$$

with the single-particle moment $Q_{\rm sp}$. Hence, in the extreme single-j configuration picture a linear trend in quadrupole moments is expected as a function of n. It reverses its sign at the middle of the orbital and for $n = 2j$ has the opposite sign, but the same absolute value as for $n = 1$. This behavior differs from that of the magnetic dipole moment which is independent of n in absolute magnitude as well as in sign. Analogously to the magnetic moments, an additivity rule can be applied for odd-odd nuclei in the weak coupling regime [2]:

$$Q(I) = \begin{pmatrix} I & 2 & I \\ -I & 0 & I \end{pmatrix}(-1)^{I_\pi+I_\nu+I}(2I+1) \times\left[\begin{Bmatrix} I_\pi & I & I_\nu \\ I & I_\pi & 2 \end{Bmatrix}\frac{Q(I_\pi)}{\begin{pmatrix} I_\pi & 2 & I_\pi \\ -I_\pi & 0 & I_\pi \end{pmatrix}} + \begin{Bmatrix} I_\nu & I & I_\pi \\ I & I_\nu & 2 \end{Bmatrix}\frac{Q(I_\nu)}{\begin{pmatrix} I_\nu & 2 & I_\nu \\ -I_\nu & 0 & I_\nu \end{pmatrix}}\right], \tag{7}$$

involving Wigner-3j and Wigner-6j symbols.

B. Large-scale shell-model calculations

For a more detailed theoretical understanding we have performed realistic shell-model calculations using the shell-model code KSHELL [39].

As shown in Fig. 4 in magenta, we consider ^{132}Sn as a closed core and let the valence protons occupy the single-particle orbitals of the $Z = 50$–82 shell ($0g_{7/2}$, $1d_{5/2}$, $1d_{3/2}$, $2s_{1/2}$, and $0h_{11/2}$) and let the valence neutrons occupy the orbitals of the $N = 82$–126 shell ($0h_{9/2}$, $1f_{7/2}$, $1f_{5/2}$, $2p_{3/2}$, $2p_{1/2}$, and $0i_{13/2}$). The starting point to construct the effective shell-model Hamiltonian is the high-precision CD-Bonn nucleon-nucleon potential [40] for which the short-range repulsive components are renormalized by the so-called Vlow−k approach [41]. This method provides a smooth potential that preserves the low-energy physics properties of the original potential and can be employed directly in the many-body perturbation theory. The low-momentum potential, with the addition of the Coulomb force for protons, is then used to derive the two-body matrix elements for the effective Hamiltonian within the framework of the $\hat{Q}$-box-plus-folded-diagram method [42,43], where the $\hat{Q}$ box is expressed as a perturbative diagrammatic expansion. The one-body matrix elements of the Hamiltonian, instead, have been taken, where possible, from experiment (see Ref. [8] for details). This effective Hamiltonian was already applied in several other studies of neutron-rich nuclei beyond ^{132}Sn [44].

For the calculation of the electromagnetic moments, we have adopted microscopic as well as empirical effective operators. The microscopic $M1$ and $E2$ effective operators are constructed consistently with the derivation of the effective Hamiltonian, by resorting to the Suzuki-Okamoto formalism [45,46], an extension of the $\hat{Q}$-box-plus-folded-diagram approach for transition operators. For the empirical magnetic dipole operator, we have used $g_l^{\rm eff}(p) = 1.18$, $g_l^{\rm eff}(n) = 0$, and $g_s^{\rm eff}(p,n) = 0.7g_s(p,n)$, where the effective neutron g factors are taken from Ref. [8] while the proton ones are fixed so as to reproduce the magnetic moment of the $7/2^+$ state in ^{133}Sb. For the electric quadrupole operator, the same effective charges of Ref. [8], $e_p^{\rm eff} = 1.7e$ and $e_n^{\rm eff} = 0.7e$, have been adopted.

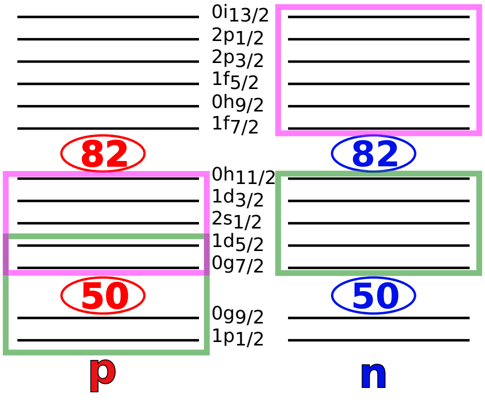

FIG. 4. Relevant orbitals for the shell-model calculations. The model space for calculations with a ^{132}Sn core is indicated by magenta rectangles, while the one for a ^{88}Sr core is defined by green rectangles.

In order to check the dependence of the theoretical moments of $N = 82$ isotones with respect to proton core excitations, we have also performed calculations by assuming $^{88}_{38}$Sr as core, with a valence space spanned by the proton orbitals $1p_{1/2}$, $0g_{9/2}$, $0g_{7/2}$, and $1d_{5/2}$ and the neutron orbitals $0g_{7/2}$, $1d_{5/2}$, $1d_{3/2}$, $2s_{1/2}$, and $0h_{11/2}$ (see Fig. 4). In this case, the effective Hamiltonian is taken from Ref. [47], where all details about its derivation can be found. Here, we only mention that it is obtained through the double-step procedure outlined in Ref. [47]. Namely, by following the procedure described above, we have derived the effective Hamiltonian in a larger model space including the $1d_{3/2}$, $2s_{1/2}$, and $0h_{11/2}$ proton orbitals. Then, by applying a unitary transformation we have computed the Hamiltonian in the truncated space. In the calculations with ^{88}Sr as a core, we have used only empirical effective operators. The adopted values for the proton g factors are $g_l^{\rm eff}(p) = 1.065$ and $g_s^{\rm eff}(p) = 0.7g_s(p)$ and for the proton effective charge $e_p^{\rm eff} = 1.6e$, neutrons being ineffective since the corresponding model space is completely filled.

V. DISCUSSION

A. $N = 82$ isotones

Figure 5 shows magnetic and quadrupole moments of the $7/2^+$ state in ^{133}Sb and higher mass isotones. As already discussed in Ref. [3], there is a large offset of the magnetic moment of ^{133}Sb to the Schmidt moment as shown in Fig. 5(a). This discrepancy was attributed to meson-exchange currents and first-order core polarization. By including higher mass isotones in the discussion, a trend towards the Schmidt value with increasing Z up to La is observed. A similar trend is known to exist for $N = 126$ isotones above Pb with protons occupying the $0h_{9/2}$ orbital [2]. There, the spin-orbit partners $0h_{9/2}$ and $0h_{11/2}$ are also stretched across the shell closure, analogously to the $0g_{7/2}$ and $0g_{9/2}$ orbitals in the $N = 82$ isotones discussed here (see Fig. 4). The decrease in magnetic moments towards the Schmidt moment with increasing Z could be qualitatively explained in part by Pauli blocking of core polarization. An increased occupancy of the $0g_{7/2}$ orbital reduces the probability of core excitations from $0g_{9/2}$ to $0g_{7/2}$ and thus limits the effect from core polarization. ^{141}Pr does not seem to follow the general trend, but its experimental uncertainty is too large for firm conclusions.

From the comparison between the experimental magnetic moments and the shell-model results based on a ^{132}Sn core, two observations can be made. First, the microscopic $M1$ operator yields results closer to the Schmidt line deviating by a factor of about 1.5 to experimental values. This might be a consequence of the strong renormalization of the $M1$ operator induced by the missing spin-orbit partner of the $0g_{7/2}$ orbital, which is only partially taken into account by our perturbative calculation. This hypothesis is supported by the magnetic moment of the $I^\pi = 5/2^+$ ground state in ^{141}Pr in Fig. 5(c), the structure of which is mostly unrelated to a $j = l \pm s$ configuration across a closed shell. Here, the calculation with the microscopic $M1$ operator agrees with experiment within 5%. Moreover, the magnetic moment of ^{133}Sn was also accurately reproduced with the same calculation method [8].

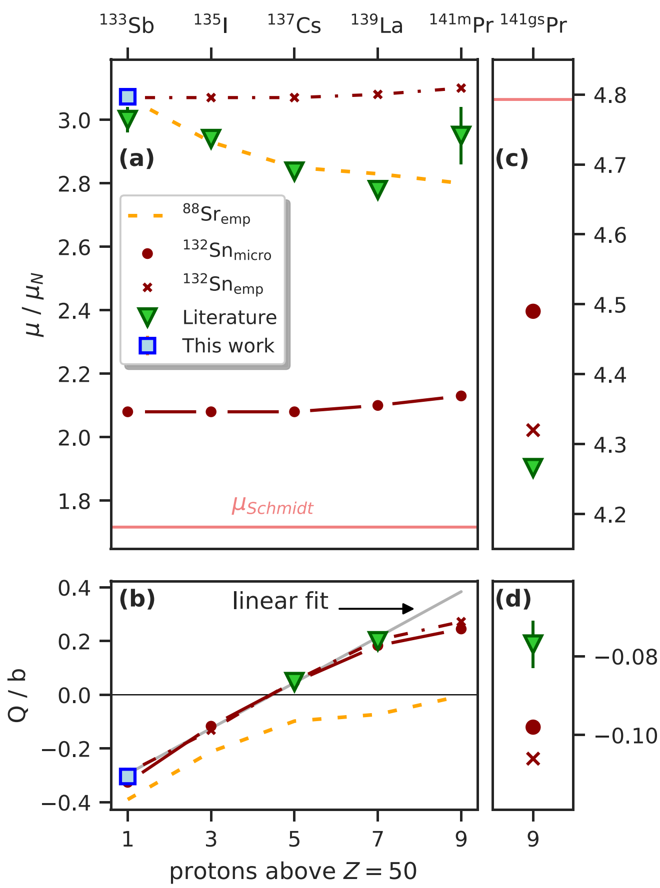

FIG. 5. (a) Magnetic and (b) quadrupole moments of ^{133}Sb and its higher mass isotones in the $7/2^+$ state compared to shell-model calculations using once a ^{132}Sn core with microscopic (^{132}Sn$_{\rm micro}$) and empirical (^{132}Sn$_{\rm emp}$) effective $M1$ and $E2$ operators and once a ^{88}Sr core with empirical operators (^{88}Sr$_{\rm emp}$). The solid line indicates the Schmidt moment of the (a) $0g_{7/2}$ and (c) $d_{5/2}$ orbital. (b) The linear fit (solid gray line) was obtained solely from experimental data. (c, d) Electromagnetic moments of the $5/2^+$ ground state of ^{141}Pr. Note the different scaling on the y axis here. Literature values taken from Refs. [3,31,48–57].

The second observation from Fig. 5(a) is that the theoretical results follow approximately a horizontal line over proton number, which does not reflect the experimental trend. In order to understand if this discrepancy arises from proton excitation across the $Z = 50$ shell closure, additional calculations with ^{88}Sr as a core were carried out, which include the $\pi 0g_{9/2}$ orbital (see again Fig. 4). As shown in Fig. 5(a), the obtained magnetic moments follow closely the experimental trend, indicating that contributions arising from the $0g_{9/2}$ orbital are essential to reproduce the experimental behavior up to La. The number of proton holes in the $0g_{9/2}$ orbital decreases slightly from Sb to Pr as visualized in Fig. 6. Note that holes in the $0g_{9/2}$ orbital are only shown indirectly by a proton occupation above the nominal occupation number. Despite their very small share of the proton occupation, these holes can have a big impact on magnetic moments due to the large value of the $\langle 0g_{9/2}|M1|0g_{7/2}\rangle$ matrix element. However, calculations with ^{88}Sr as a core do not reproduce the rise of

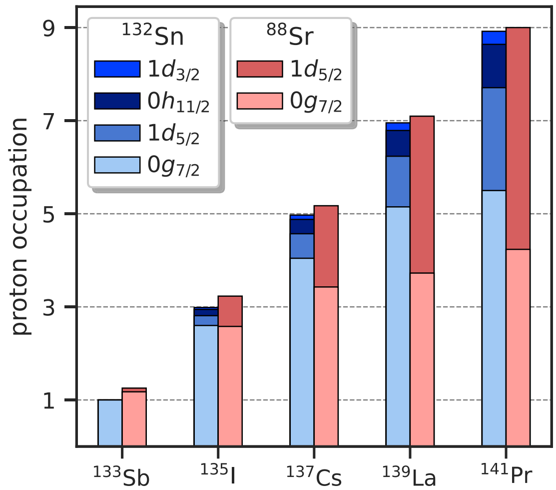

FIG. 6. Proton occupation of the orbitals in the $Z = 50$–82 shell for the yrast $7/2^+$ state in $N = 82$ isotones, obtained from ^{132}Sn-core and ^{88}Sr-core calculations. Values above the nominal proton occupation (1, 3, 5, 7, and 9) for the ^{88}Sr core arise due to holes in the $0g_{9/2}$ orbital. Note that the model space of the ^{88}Sr calculations does not include orbitals above $1d_{5/2}$. Contributions from the $2s_{1/2}$ and $1p_{1/2}$ orbitals are negligible for ^{132}Sn and ^{88}Sr as core, respectively, and are thus not shown in the figure. In the employed model spaces the neutron orbitals are empty (full) and can be therefore neglected.

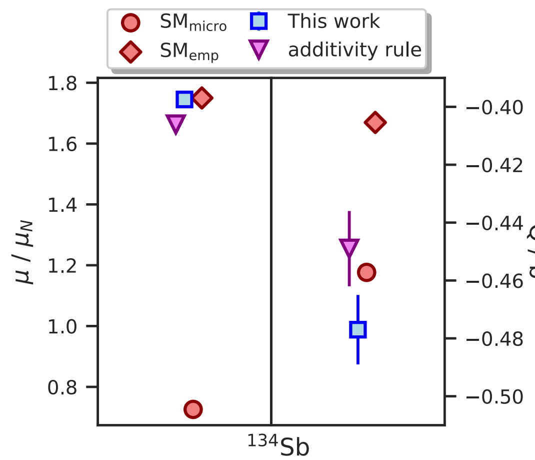

FIG. 7. Magnetic and quadrupole moments of ^{134}Sb compared to shell-model calculations with ^{132}Sn as core and the additivity rule [Eq. (5)]. For the additivity rule, the experimental moments from ^{133}Sb and ^{133}Sn [8] were taken for the proton and neutron contribution, respectively.

the magnetic moment in Pr. This is most likely due the omission of the $0h_{11/2}$ orbital, which gives a positive contribution as observed in calculations with ^{132}Sn as core (see Figs. 5 and 6).

The experimental results for the quadrupole moments of the $N = 82$ isotones are shown in Fig. 5(b). They follow a linearly increasing trend over proton number, which can be easily explained by the seniority scheme [see Eq. (6)]. Around closed shells, an orbital occupied by a single particle is expected to result in a negative quadrupole moment and thus an oblate shape. This is indeed the case for ^{133}Sb with a single proton in the $0g_{7/2}$ orbital, while the neutron shell is closed. By filling up the $0g_{7/2}$ orbital, the nucleus should transform to a prolate shape with positive quadrupole moment and cross $Q = 0$ (i.e., spherical shape) at a half-filled orbital. Hence, the trend seen in Fig. 5(b) can be described qualitatively in such a simplistic picture, indicated by a linear fit. Similar trends have been observed for instance along the $\nu 0f_{7/2}$ and $\nu 1p_{3/2}$ orbitals of Ca [58] as well as the $\nu 0h_{11/2}$ and $\nu 1d_{3/2}$ orbitals in Cd [59] and Sn [60], respectively.

The quadrupole moments calculated within the shell model using a ^{132}Sn core are in very good agreement with the experiment, where microscopic and empirical operators deliver equally good results. This shows that, in contrast to the microscopic $M1$ operator, the $E2$ operator seems to be insensitive to the explicit presence of the $0g_{9/2}$ orbital in the model space. The fact that the linear fit in Fig. 5(b) does not cross $Q = 0$ in the middle of the $0g_{7/2}$ can be attributed to contributions from higher-lying orbitals. These may be seen by looking at the proton occupation as shown in Fig. 6. The $0g_{7/2}$ orbital includes the major share of the proton configuration, but, with increasing Z, contributions from $1d_{5/2}$ and $0h_{11/2}$ also rise. The occupation of the $0g_{7/2}$ orbital increases only slightly in $^{141\rm m}$Pr compared to ^{139}La while higher-lying orbitals receive the largest portion of the additional two protons. Therefore, the quadrupole moment of the $I^\pi = 7/2^+$ isomer in ^{141}Pr is quite close to that of the ground state in ^{139}La, which is dominated by a one-hole configuration in the $0g_{7/2}$ orbital.

Unlike the magnetic moments, the ^{88}Sr-core calculations lead to larger discrepancies between theoretical and experimental quadrupole moments as shown in Fig. 5(b). In particular, they do not reproduce the correct sign for heavier isotones. From the analysis of the wave functions we have found that the missing contributions from $1d_{3/2}$, $2s_{1/2}$, and $0h_{11/2}$ orbitals, which are outside the model space of our ^{88}Sr calculations, are responsible for such discrepancies. Actually, a more complete description of the nuclei under investigation would require the inclusion of these proton orbitals in addition to the ones below the $Z = 50$ shell closure. This would lead to quite a large model space, which is very demanding from a computational point of view.

B. ^{134}Sb

In a simplistic view, ^{134}Sb can be understood as the sum of the valence proton of ^{133}Sb in the $0g_{7/2}$ orbital and the valence neutron of ^{133}Sn in the $1f_{7/2}$ orbital. Indeed, as shown in Fig. 7, the additivity rules for the electromagnetic moments [see Eqs. (5) and (7)] provide a very good agreement with the new experimental data for the $I = (7^-)$ isomer in ^{134}Sb when the measured moments of ^{133}Sb and ^{133}Sn are used.

Evidence of the validity of the additivity rule emerges also from shell-model calculations (performed with a ^{132}Sn core). These predict for the 7^- state the dominant $\pi 0g_{7/2} \times \nu 1f_{7/2}$ maximally aligned configuration, which accounts for almost 100% of the wave function. Consequently, the theoretical dipole and quadrupole moments of this state, obtained with both empirical and microscopic operators, are very close to those computed by summing the theoretical moments of the

$7/2^+$ state in ^{133}Sb and of the $7/2^-$ state in ^{133}Sn. As shown in Fig. 7, shell-model calculations reproduce very well the experimental magnetic moment of the (7^-) isomeric state in ^{134}Sb once the empirical g factors are adopted, while a good agreement with the experiment is obtained for the quadrupole moments by using both empirical and microscopic approaches, deviating by 15% at most.

Applying the additivity rule to the calculated magnetic moments from the microscopic approach of ^{133}Sb and ^{133}Sn yields almost the same value for ^{134}Sb as the shell-model calculations. Hence, the large underestimation of the experimental magnetic moment by the microscopic approach with a factor >2 is solely caused by the disagreement of the calculated moment of ^{133}Sb [see Fig. 5(a)].

VI. CONCLUSION

Electromagnetic moments of the $7/2^+$ ground state in ^{133}Sb and the (7^-) isomer ^{134}Sb were determined by collinear laser spectroscopy. These observables provide new insights into single-particle behavior of nuclides above the doubly magic nucleus ^{132}Sn.

Experimental quadrupole moments of $N = 82$ isotones with a valence proton in the $0g_{7/2}$ orbital follow a linear trend with respect to the proton number up to ^{139}La. Therefore, they represent a textbook example for the application of the seniority scheme to the filling of the $0g_{7/2}$ orbital. In contrast, experimental magnetic moments, in addition to being rather far from the Schmidt values, deviate from the constant behavior predicted by the seniority scheme, thus indicating the sensitivity to more complex phenomena.

In order to interpret the data, we have performed shell-model calculations with ^{132}Sn as a closed core and employed microscopic and empirical operators for computing electromagnetic properties. The theoretical results with both operators are in very good agreement with the experimental data for the quadrupole moments, while they fail in reproducing the experimental behavior of the magnetic moments. Moreover, the use of a microscopic $M1$ operator yields magnetic moments that are very close to the Schmidt line, and which largely underestimate the experimental value. These deviations may be related to $M1$ core-polarization excitations, also observed above the doubly magic ^{208}Pb, and especially to the lack of the $M1$ spin-flip $0g_{9/2} \rightarrow 0g_{7/2}$ transition in our model space.

In light of these results, we have carried out shell-model calculations by considering a ^{88}Sr core, including the $0g_{9/2}$ and $1p_{1/2}$ proton orbitals below $Z = 50$. Indeed, these calculations reproduce the experimental magnetic moments very well. However, the ^{88}Sr model space misses important contributions from $1d_{3/2}$, $2s_{1/2}$, and $0h_{11/2}$ proton orbitals, leading to a disagreement in the quadrupole moments. An ideal model space in this region of the nuclear chart, that reproduced both magnetic and quadrupole moments equally well, would require the inclusion of the proton $0g_{9/2}$ orbital as well as of the whole $Z = 50$–82 shell. This is however rather cumbersome from a computational point of view.

On the other hand, ^{134}Sb is easier to interpret and constitutes another textbook example. In this case, the additivity rule for odd-odd nuclei gives excellent agreement with the experiment. These results are supported by shell-model calculations revealing a pure configuration of the proton in the $0g_{7/2}$ and the neutron in the $1f_{7/2}$ orbital above a ^{132}Sn core.

ACKNOWLEDGMENTS

We would like to thank the ISOLDE collaboration and the ISOLDE technical teams for supporting the preparation and the successful realization of the experiment. This work was supported by BriX Research Program No. P7/12, FWO-Vlaanderen (Belgium), KU Leuven Grant No. GOA 15/010, UK Science and Technology Facilities Council Grants No. ST/L005794/1 and No. ST/P004598/1, National Science Foundation Grant No. PHY-1068217, Federal Ministry of Education and Research Contract No. 05P18RDCIA, the Max-Planck Society, the Helmholtz International Center for FAIR, National Key Research and Development Program of China Grant No. 2018YFA0404403, National Natural Science Foundation of China Grants No. 11875073 and No. U1967201), and the EU Horizon 2020 research and innovation program through ENSAR2 (Grant No. 654002). We acknowledge the CINECA award under the ISCRA initiative code HP10B51E4M and through the INFN-CINECA agreement for the availability of high performance computing resources and support. G.D.G. acknowledges support by the funding program VALERE of Università degli Studi della Campania Luigi Vanvitelli.

[1] M. Thoennessen, 2018 update of the discoveries of nuclides, Int. J. Mod. Phys. E **28**, 1930002 (2019).

[2] G. Neyens, Nuclear magnetic and quadrupole moments for nuclear structure research on exotic nuclei, Rep. Prog. Phys. **66**, 633 (2003).

[3] N. J. Stone, D. Doran, M. Lindroos, J. Rikovska, M. Veskovic, G. White, D. A. Williams, B. Fogelberg, L. Jacobsson, I. S. Towner, and K. Heyde, Magnetic Moments of Odd-A Sb Isotopes to ^{133}Sb: Significant Evidence for Mesonic Exchange Current Contributions and on Core Collective g Factors, Phys. Rev. Lett. **78**, 820 (1997).

[4] T. Ohtsubo, N. J. Stone, J. R. Stone, I. S. Towner, C. R. Bingham, C. Gaulard, U. Köster, S. Muto, J. Nikolov, K. Nishimura, G. S. Simpson, G. Soti, M. Veskovic, W. B. Walters, and F. Wauters, Magnetic Dipole Moment of the Doubly-Closed-Shell Plus One Proton Nucleus ^{49}Sc, Phys. Rev. Lett. **109**, 032504 (2012).

[5] P. Vingerhoets, K. T. Flanagan, M. Avgoulea, J. Billowes, M. L. Bissell, K. Blaum, B. A. Brown, B. Cheal, M. De Rydt, D. H. Forest, C. Geppert, M. Honma, M. Kowalska, J. Krämer, A. Krieger, E. Mané, R. Neugart, G. Neyens, W. Nörtershäuser, T. Otsuka *et al.*, Nuclear spins, magnetic moments, and

quadrupole moments of Cu isotopes from $N = 28$ to $N = 46$: Probes for core polarization effects, Phys. Rev. C **82**, 064311 (2010).

[6] K. L. Jones, A. S. Adekola, D. W. Bardayan, J. C. Blackmon, K. Y. Chae, K. A. Chipps, J. A. Cizewski, L. Erikson, C. Harlin, R. Hatarik, R. Kapler, R. L. Kozub, J. F. Liang, R. Livesay, Z. Ma, B. H. Moazen, C. D. Nesaraja, F. M. Nunes, S. D. Pain, N. P. Patterson *et al.*, The magic nature of ^{132}Sn explored through the single-particle states of ^{133}Sn, Nature (London) **465**, 454 (2010).

[7] J. M. Allmond, A. E. Stuchbery, J. R. Beene, A. Galindo-Uribarri, J. F. Liang, E. Padilla-Rodal, D. C. Radford, R. L. Varner, A. Ayres, J. C. Batchelder, A. Bey, C. R. Bingham, M. E. Howard, K. L. Jones, B. Manning, P. E. Mueller, C. D. Nesaraja, S. D. Pain, W. A. Peters, A. Ratkiewicz *et al.*, Double-Magic Nature of ^{132}Sn and ^{208}Pb Through Lifetime and Cross-Section Measurements, Phys. Rev. Lett. **112**, 172701 (2014).

[8] L. V. Rodríguez, D. L. Balabanski, M. L. Bissell, K. Blaum, B. Cheal, G. De Gregorio, J. Ekman, R. F. Garcia Ruiz, A. Gargano, G. Georgiev, W. Gins, C. Gorges, H. Heylen, A. Kanellakopoulos, S. Kaufmann, V. Lagaki, S. Lechner, B. Maaß, S. Malbrunot-Ettenauer, R. Neugart *et al.*, Doubly-magic character of ^{132}Sn studied via electromagnetic moments of ^{133}Sn, Phys. Rev. C **102**, 051301(R) (2020).

[9] R. Catherall, W. Andreazza, M. Breitenfeldt, A. Dorsival, G. J. Focker, T. P. Gharsa, T. J. Giles, J.-L. Grenard, F. Locci, P. Martins, S. Marzari, J. Schipper, A. Shornikov, and T. Stora, The ISOLDE facility, J. Phys. G **44**, 094002 (2017).

[10] V. Fedosseev, K. Chrysalidis, T. D. Goodacre, B. Marsh, S. Rothe, C. Seiffert, and K. Wendt, Ion beam production and study of radioactive isotopes with the laser ion source at ISOLDE, J. Phys. G **44**, 084006 (2017).

[11] H. Frånberg, P. Delahaye, J. Billowes, K. Blaum, R. Catherall, F. Duval, O. Gianfrancesco, T. Giles, A. Jokinen, M. Lindroos, D. Lunney, E. Mane, and I. Podadera, Off-line commissioning of the ISOLDE cooler, Nucl. Instrum. Methods B **266**, 4502 (2008).

[12] R. Neugart, J. Billowes, M. L. Bissell, K. Blaum, B. Cheal, K. T. Flanagan, G. Neyens, W. Nörtershäuser, and D. T. Yordanov, Collinear laser spectroscopy at ISOLDE: New methods and highlights, J. Phys. G **44**, 064002 (2017).

[13] A. Mueller, F. Buchinger, W. Klempt, E. Otten, R. Neugart, C. Ekström, and J. Heinemeier, Spins, moments and charge radii of barium isotopes in the range $^{122-146}$Ba determined by collinear fast-beam laser spectroscopy, Nucl. Phys. A **403**, 234 (1983).

[14] A. Klose, K. Minamisono, C. Geppert, N. Frömmgen, M. Hammen, J. Krämer, A. Krieger, C. Levy, P. Mantica, W. Nörtershäuser, and S. Vinnikova, Tests of atomic charge-exchange cells for collinear laser spectroscopy, Nucl. Instrum. Methods A **678**, 114 (2012).

[15] S. Kaufman, High-resolution laser spectroscopy in fast beams, Opt. Commun. **17**, 309 (1976).

[16] A. Nieminen, P. Campbell, J. Billowes, D. H. Forest, J. A. R. Griffith, J. Huikari, A. Jokinen, I. D. Moore, R. Moore, G. Tungate, and J. Äystö, On-Line Ion Cooling and Bunching for Collinear Laser Spectroscopy, Phys. Rev. Lett. **88**, 094801 (2002).

[17] E. Mané, B. Cheal, J. Billowes, M. L. Bissell, K. Blaum, F. C. Charlwood, K. T. Flanagan, D. H. Forest, C. Geppert, M. Kowalska, A. Krieger, J. Krämer, I. D. Moore, R. Neugart, G. Neyens, W. Nörtershäuser, M. M. Rajabali, R. Sánchez, M. Schug, H. H. Stroke *et al.*, Ground-state spins and moments of ^{72,74,76,78}Ga nuclei, Phys. Rev. C **84**, 024303 (2011).

[18] W. Gins, R. de Groote, M. Bissell, C. G. Buitrago], R. Ferrer, K. Lynch, G. Neyens, and S. Sels, Analysis of counting data: Development of the SATLAS Python package, Comput. Phys. Commun. **222**, 286 (2018).

[19] R. Neugart, S. L. Kaufman, W. Klempt, G. Moruzzi, E.-W. Otten, and B. Schinzler, High-resolution spectroscopy in fast atomic beams, in *Laser Spectroscopy III*, edited by J. L. Hall and J. L. Carlsten (Springer-Verlag, Berlin, 1977), pp. 446–447.

[20] N. Bendali, H. T. Duong, P. Juncar, J. M. S. Jalm, and J. L. Vialle, Na^+-Na charge exchange processes studied by collinear laser spectroscopy, J. Phys. B **19**, 233 (1986).

[21] P. C. B. Fernando, G. K. Rochester, I. J. Spalding, and K. F. Smith, The hyperfine structure of ^{121}Sb and ^{123}Sb, Philos. Mag. **5**, 1291 (1960).

[22] J. Eisinger and G. Feher, HFS anomaly of Sb^{121} and Sb^{123} determined by the electron nuclear double resonance technique, Phys. Rev. **109**, 1172 (1958).

[23] S. Büttgenbach, Magnetic hyperfine anomalies, Hyperfine Interact. **20**, 1 (1984).

[24] S. Lechner, Laser spectroscopy of antimony isotopes and the design of a cryogenic paul trap, Ph.D thesis, submitted at TU Wien, 2021.

[25] A. Kramida, Yu. Ralchenko, J. Reader, and NIST ASD Team, NIST Atomic Spectra Database (version 5.8), National Institute of Standards and Technology, Gaithersburg, MD, 2020, 28 March 2021.

[26] G. Bocchi, S. Leoni, B. Fornal, G. Col'o, P. Bortignon, S. Bottoni, A. Bracco, C. Michelagnoli, D. Bazzacco, A. Blanc, G. de France, M. Jentschel, U. Köster, P. Mutti, J.-M. Régis, G. Simpson, T. Soldner, C. Ur, W. Urban, L. Fraile *et al.*, The mutable nature of particle-core excitations with spin in the one-valence-proton nucleus ^{133}*Sb*, Phys. Lett. B **760**, 273 (2016).

[27] J. Shergur, A. Wöhr, W. B. Walters, K.-L. Kratz, O. Arndt, B. A. Brown, J. Cederkall, I. Dillmann, L. M. Fraile, P. Hoff, A. Joinet, U. Köster, and B. Pfeiffer, Level structure of odd-odd ^{134}Sb populated in the β^- decays of ^{134,135}Sn, Phys. Rev. C **71**, 064321 (2005).

[28] F. Hassini, Z. B. Ahmed, O. Robaux, J. Vergès, and J.-F. Wyart, Study of fine and hyperfine structures in the spectrum of neutral antimony (^{121}Sb I), J. Opt. Soc. Am. B **5**, 2060 (1988).

[29] L. Sobolewski, S. Bouazza, and J. Kwela, Fine, hyperfine and zeeman structures of levels of ^{123}Sb I, European Phys. J. D **70** (2016).

[30] R. L. A. Haiduke, A. B. F. da Silva, and L. Visscher, The nuclear electric quadrupole moment of antimony from the molecular method, J. Chem. Phys. **125**, 064301 (2006).

[31] N. Stone, Table of recommended nuclear magnetic dipole moments, INDC(NDS)-0794, INDC International Nuclear Data Committee (2019).

[32] W. G. Proctor and F. C. Yu, On the nuclear magnetic moments of several stable isotopes, Phys. Rev. **81**, 20 (1951).

[33] Y. Koi, M. Kawakami, T. Hihara, and A. Tsujimura, Hyperfine fields at P^{31}, As^{75}, Nb^{93}, Sb^{121} and Sb^{123} in iron, J. Phys. Soc. Jpn. **33**, 267 (1972).

[34] P. Callaghan, M. Shott, and N. Stone, The magnetic dipole moments of doubly odd antimony isotopes with $(h_{112})n$ neutron configuration, Nucl. Phys. A **221**, 1 (1974).

[35] I. Talmi, The shell model—simplicity from complexity: Some of my best nuclei are spherical, Phys. Scr. **92**, 083001 (2017).

[36] G. Schneider, A. Mooser, M. Bohman, N. Schön, J. Harrington, T. Higuchi, H. Nagahama, S. Sellner, C. Smorra, K. Blaum, Y. Matsuda, W. Quint, J. Walz, and S. Ulmer, Double-trap measurement of the proton magnetic moment at 0.3 parts per billion precision, Science **358**, 1081 (2017).

[37] E. Tiesinga, P. J. Mohr, D. B. Newell, and B. N. Taylor, The 2018 CODATA recommended values of the fundamental physical constants (version 8.1), National Institute of Standards and Technology, Gaithersburg (2020).

[38] R. F. Casten, *Nuclear Structure from a Simple Perspective*, 2nd ed. (Oxford University Press, New York, 2001).

[39] N. Shimizu, T. Mizusaki, Y. Utsuno, and Y. Tsunoda, Thick-restart block Lanczos method for large-scale shell-model calculations, Comput. Phys. Commun. **244**, 372 (2019).

[40] R. Machleidt, High-precision, charge-dependent Bonn nucleon-nucleon potential, Phys. Rev. C **63**, 024001 (2001).

[41] S. Bogner, T. T. S. Kuo, L. Coraggio, A. Covello, and N. Itaco, Low momentum nucleon-nucleon potential and shell model effective interactions, Phys. Rev. C **65**, 051301(R) (2002).

[42] L. Coraggio, A. Covello, A. Gargano, N. Itaco, and T. Kuo, Shell-model calculations and realistic effective interactions, Prog. Part. Nucl. Phys. **62**, 135 (2009).

[43] L. Coraggio, A. Covello, A. Gargano, N. Itaco, and T. Kuo, Effective shell-model Hamiltonians from realistic nucleon-nucleon potentials within a perturbative approach, Ann. Phys. (NY) **327**, 2125 (2012).

[44] B. F. Bayman, A. Covello, A. Gargano, P. Guazzoni, and L. Zetta, Two-neutron transfer in Sn isotopes beyond the $N = 82$ shell closure, Phys. Rev. C **90**, 044322 (2014).

[45] K. Suzuki and R. Okamoto, Effective operators in time-independent approach, Prog. Theor. Phys. **93**, 905 (1995).

[46] L. Coraggio, L. De Angelis, T. Fukui, A. Gargano, N. Itaco, and F. Nowacki, Renormalization of the Gamow-Teller operator within the realistic shell model, Phys. Rev. C **100**, 014316 (2019).

[47] L. Coraggio, A. Gargano, and N. Itaco, Double-step truncation procedure for large-scale shell-model calculations, Phys. Rev. C **93**, 064328 (2016).

[48] G. White, N. Stone, J. Rikovska, S. Ohya, J. Copnell, T. Giles, Y. Koh, I. Towner, B. Brown, B. Fogelberg, L. Jacobsson, P. Rahkila, and M. Hjorth-Jensen, Magnetic dipole moments near ^{132}Sn: New measurement on ^{135}I by NMR/ON, Nucl. Phys. A **644**, 277 (1998).

[49] H. H. Stroke, V. Jaccarino, D. S. Edmonds, and R. Weiss, Magnetic moments and hyperfine-structure anomalies of Cs^{133}, Cs^{134}, Cs^{135}, and Cs^{137}, Phys. Rev. **105**, 590 (1957).

[50] F. Ackermann, E. Otten, G. zu Putlitz, A. Schenck, and S. Ullrich, Determination of the spectroscopic quadrupole moments of ^{131}Cs, ^{132}Cs and ^{136}Cs, Nucl. Phys. A **248**, 157 (1975).

[51] H. Krüger, O. Lutz, and H. Oehler, Nuclear magnetic moments and ratios of quadrupole moments ^{135}Ba, ^{137}Ba, ^{138}La, ^{139}La by NMR spectroscopy, Phys. Lett. A **62**, 131 (1977).

[52] C. R. Jacob, L. Visscher, C. Thierfelder, and P. Schwerdtfeger, Nuclear quadrupole moment of ^{139}La from relativistic electronic structure calculations of the electric field gradients in LaF, LaCl, LaBr, and LaI, J. Chem. Phys. **127**, 204303 (2007).

[53] J. G. Stevens and B. D. Dunlap, Nuclear moments and moment ratios as determined by Mössbauer spectroscopy, J. Phys. Chem. Ref. Data **5**, 1093 (1976).

[54] R. M. Macfarlane, D. P. Burum, and R. M. Shelby, New Determination of the Nuclear Magnetic Moment of ^{141}Pr, Phys. Rev. Lett. **49**, 636 (1982).

[55] H. Iimura, Y. Nakahara, S. Ichikawa, M. Kubota, and T. Horiguchi, Nuclear moments of ^{143}Pr by laser spectroscopy, Phys. Rev. C **50**, 661 (1994).

[56] N. Stone, Table of nuclear magnetic dipole and electric quadrupole moments, INDC(NDS)-0658, INDC International Nuclear Data Committee (2014).

[57] N. Stone, Table of nuclear electric quadrupole moments, At. Data Nucl. Data Tables **111–112**, 1 (2016).

[58] R. F. Garcia Ruiz, M. L. Bissell, K. Blaum, N. Frömmgen, M. Hammen, J. D. Holt, M. Kowalska, K. Kreim, J. Menéndez, R. Neugart, G. Neyens, W. Nörtershäuser, F. Nowacki, J. Papuga, A. Poves, A. Schwenk, J. Simonis, and D. T. Yordanov, Ground-state electromagnetic moments of calcium isotopes, Phys. Rev. C **91**, 041304(R) (2015).

[59] D. T. Yordanov, D. L. Balabanski, J. Bieroń, M. L. Bissell, K. Blaum, I. Budinčević, S. Fritzsche, N. Frömmgen, G. Georgiev, C. Geppert, M. Hammen, M. Kowalska, K. Kreim, A. Krieger, R. Neugart, W. Nörtershäuser, J. Papuga, and S. Schmidt, Spins, Electromagnetic Moments, and Isomers of $^{107-129}$Cd, Phys. Rev. Lett. **110**, 192501 (2013).

[60] D. T. Yordanov, L. V. Rodríguez, D. L. Balabanski, J. Bieroń, M. L. Bissell, K. Blaum, B. Cheal, J. Ekman, G. Gaigalas, R. F. Garcia Ruiz, G. Georgiev, W. Gins, M. R. Godefroid, C. Gorges, Z. Harman, H. Heylen, P. Jönsson, A. Kanellakopoulos, S. Kaufmann, C. H. Keitel *et al.*, Structural trends in atomic nuclei from laser spectroscopy of tin, Commun. Phys. **3**, 107 (2020).